RECENT DEVELOPMENTS ON HIGH INTENSITY BEAM DIAGNOSTICS AT SNS*

W. Blokland, ORNL*, Oak Ridge, TN 37831, USA

Abstract

The Spallation Neutron Source Ring accumulates 0.6 us long proton bunches of up to 1.5e14 protons with a typical peak current of over 50 Amp during a 1 ms cycle. To qualify the beam, we perform different transverse profile measurements that can be done at full intensity. The electron beam scanner performs a non-interceptive measurement of the transverse and longitudinal profiles of the beam in the ring. Electrons passing over and through the proton beam are deflected and projected onto a fluorescent screen. Analysis of the projection yields the transverse profile while multiple transverse profiles, offset in time, yield the longitudinal profile. Progress made with this system will be discussed as well as temperature measurements of the stripper foil and the target imaging system.

INTRODUCTION

Up to a thousand proton beam bunches from the linac accumulate in the ring to generate an approx. 645 ns long proton pulse of up to 1.5e14 protons. Figure 1 shows the linac (green), the ring (blue), and the beam on target (red) current waveforms. The linac current is multiplied 100x to make it visible. The process repeats at 60 Hz.

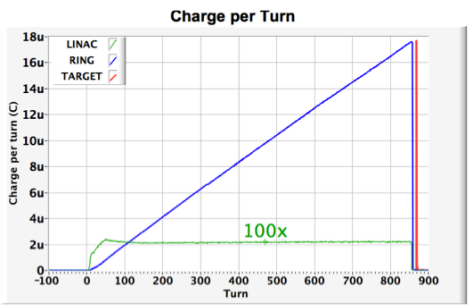

Figure 1: The accumulation of particles in the ring.

The 1 ms long accumulation of bunches in the ring with ever-increasing intensity makes it a challenging environment in which to use an interceptive device to make transverse measurements in the ring. This excludes the use of standard wire scanners at full beam power. Instead, we have one electron scanner for each plane to measure the horizontal and vertical transverse profiles [1,2]. The electron scanner for the vertical profile (horizontally mounted) is shown in Fig. 2.

* ORNL/SNS is managed by UT-Battelle, LLC, for the U.S. Department of Energy under contract DE-AC05-00OR22725

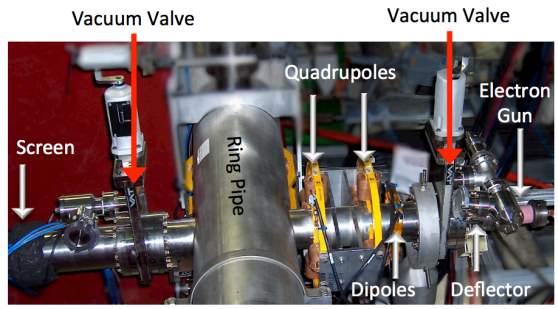

Figure 2: The electron scanner.

The Target Imaging System (TIS) makes the final transverse profile measurement. The system consists of a digital camera viewing the fluorescent coating of Cr:Al2O3 on the target. The light emanating from the coating is directed through mirrors and optical fibers to a low radiation area [3]. The latest installed target is shown in Fig. 3 with a superimposed TIS image.

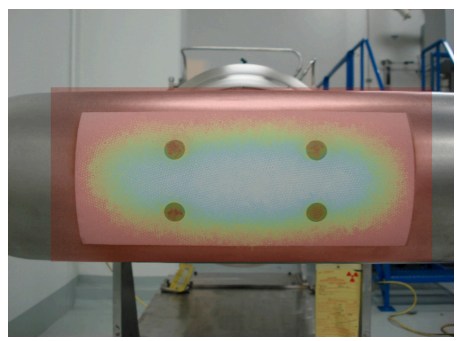

Figure 3: Target vessel with superimposed TIS image.

Another important aspect of the SNS accelerator is the stripper foil [4]. This foil strips the electrons from the H^- beam to implement a charge-exchange injection scheme. The foil must be positioned such that it strips as much of the incoming H^- beam as possible but also such that it minimizes interception of the circulating proton beam. A radiation hard analog video system installed in the tunnel provides foil images at 30 Hz or half the beam rep rate. A new telescope-based Foil Imaging System (FIS) has been installed outside of the tunnel to provide better visibility of the foil and also to make temperature measurements, see Fig. 4.

This paper presents progress made with the electron scanner, the Target Imaging System, and the Foil Imaging System.

ISBN 978-3-95450-118-2

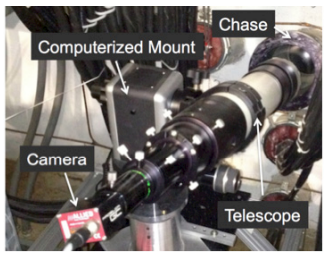

Figure 4: New optical system to observe stripping foil.

ELECTRON SCANNER

The electron scanner performs non-interceptive transverse profile scans at any point in the accumulation cycle. The profiles are derived by analyzing the deflection of the electrons due to the electro-magnetic field of the proton beam, see Fig. 5. By combining multiple scans, offset in time, the electron scanner can also show the longitudinal profile, similar to a current monitor.

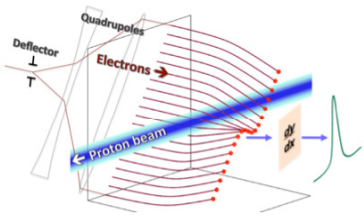

Figure 5: The proton beam deflects the electrons.

Simulation

The principles behind the electron scanner assume a constant proton beam field during the scan. The scan lasts only 20 ns, which is short enough for the ~645 ns long bunch of the SNS Ring. In collaboration with Fermilab's ProjectX, we performed simulations to see if a SNS style electron scanner can still deliver useful profiles with much shorter proton bunches. In particular, we simulated the results given a 3 ns proton bunch similar to a Fermilab Main Injector bunch while still using relatively long scan durations. To make much shorter scans, the hardware would have to be significantly upgraded, thus increasing the cost and complexity of the scanner.

The first simulation assumes a pencil electron beam steered by a deflector to scan diagonally through a transversely Gaussian shaped proton bunch of 120 GeV, 2 mm wide, and 3 ns long (also Gaussian shape) with 10e10 particles. The 20 ns long scan simulation resulted in an estimated 1.4 mm sigma, while the 3 ns scan resulted in a sigma close to 2 mm, see Fig. 6. The results show that the electron beam has to be longitudinally and transversely aligned with the proton bunch to get a near symmetric profile. However, the calculated profiles are becoming unrepresentative of the actual proton beam profile once the electron scan duration is longer than the length of the proton beam.

A second simulation assumes a non-moving electron beam as the proton beam passes by, similar to [5]. This generates a projection as shown on the left side of Fig. 7. All deflection is due to the proton beam. The right side of the figure shows the intensity distribution of the projected electrons during the proton bunch with the electron beam at an offset of 7.1 mm relative to the transverse center of the proton bunch.

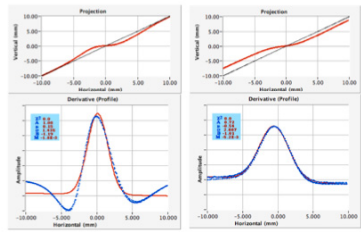

Figure 6: Simulated profiles using different duration scans.

Note that, depending on the spacing between the proton bunches, more electrons will land at the non-deflected 7.1 mm, which can give a very bright spot compared to the projected curve, thus complicating the analysis. The maximum deflection occurs during the most intense part of the proton bunch and compares to an equivalent part in an electron scan using a deflector.

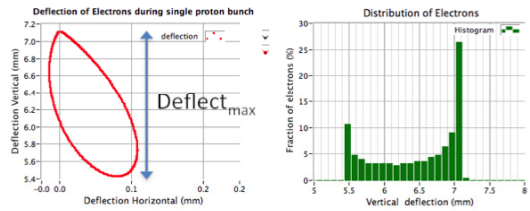

Figure 7: Deflection of the electron beam by a single proton bunch.

Figure 8 shows, on the left, the maximum deflection for each position of the electron beam relative, transversely, to the proton beam. The right part of the figure shows the reconstructed profile closely matching the Gaussian distribution used in the simulation. This method would allow using a slowly stepping electron beam to measure the profile, given a repetitive proton beam bunch.

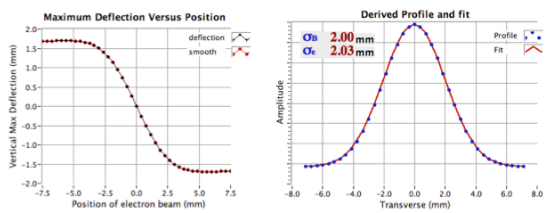

Figure 8: Maximum deflections vs. positions and the reconstructed Gaussian profile.

Image Analysis

To obtain the transverse profile of the proton beam, the analysis takes the derivative, dy/dx, of the curve points, the set of (x,y) points. A typical transverse profile in the SNS ring can be described as the sum of two super-Gaussians [6]. The super-Gaussians are fitted to the derivative to obtain a smoothed result. The model-based

ISBN 978-3-95450-118-2

approach allows us to remove the aberrations in the final display. In order to possibly improve the stability and speed up the analysis, we added the capability to fit directly to the curve points with the integral version of the sum of super-Gaussians. Integrating a super-Gaussian results in a Gamma function. Besides the two Gamma functions, the fitting function also includes a quadratic curvature to account for observed aberrations. These aberrations are thought to be due to steering the beam away from the center of the quadrupoles. This aberration is a problem especially for the vertical profiles, as its beam pipe segments were not welded straight and electrons must be steered off center to reach the screen. The final fitting function for a single super-Gaussian becomes:

$$\int \left(a \cdot e^{-0.5\left(\frac{x-\mu}{\sigma}\right)^n} + sl \cdot x + o \right) dx = a \cdot \frac{2^{\frac{1}{n}}}{n} \cdot sign\,(x-\mu) \cdot \mathrm{Gamma}\left[\frac{1}{n}, 0.5\left(\frac{x-\mu}{\sigma}\right)^n\right] + o \cdot x + \frac{sl}{2} \cdot x^2 - sl \cdot \mu \cdot x + c \quad (1)$$

To allow for a non-even power of n, the absolute value of (x-μ) is taken in the Gamma function. The fitting results are shown in Fig. 9.

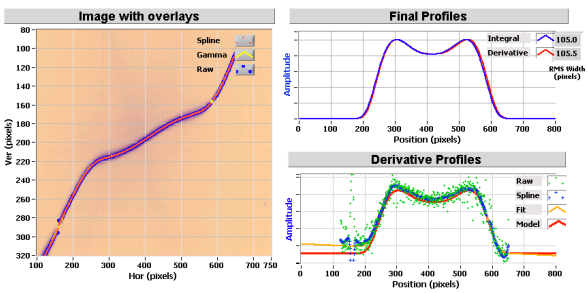

Figure 9: Example of fitting to the curve and deriving the profile.

The left of the figure shows the fitted curves superimposed on the image. The right top plot shows the profiles obtained with the derivative and integral methods. The bottom right plot shows the raw points by taking the derivative directly from the curve points, the derivative of the spline fitted to the curve points, the super-Gaussian fit with aberration to the derivative points of the spline, and the model with the aberration zeroed out. The integral and derivative methods show very similar results and stability. Unfortunately, in terms of speed, the integral method is much slower, up to a factor of ten, requiring up to 20 seconds, which is too long for use during studies.

Deflector Angle

The angles of the deflectors for both scanners are at 45 degrees. However, the tails of the profiles are barely seen by the limited range of the electron scanner, especially in case of the vertical profile. To increase the range, we rotated the deflector for the vertical profile to almost 70 degrees, see Fig. 10. The image shows that we can complete the improvement by adjusting the camera optics.

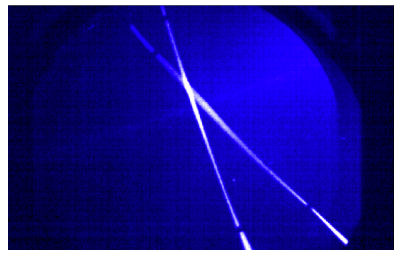

Figure 10: The electron projection at 45 degrees and the newly rotated curve of almost 70 degrees.

Figure 11 compares the vertical profiles from before the rotation (top) and after the rotation (bottom). This shows that, indeed, we can see more of the tails. One thing to keep in mind is that we have reduced our resolution, as the curve now occupies a smaller area of the screen.

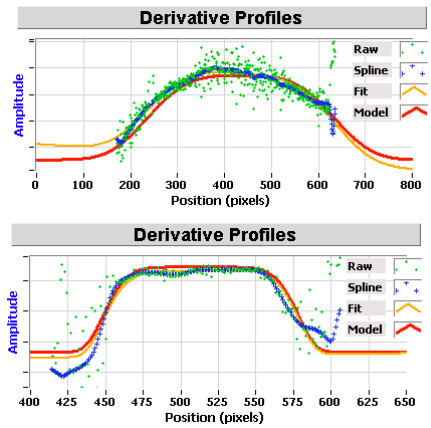

Figure 11: Above is the profile at 45 degrees and below is the profile at 65 degrees.

Cathode Performance

After rotating the vertical deflector, we found a much-reduced intensity of the electron gun. Even with focusing the beam in one spot on the screen (deflector off), a visible spot was seen for only 15 minutes, see Fig. 12. The horizontal gun (blue trace) is still warming up and increasing in intensity while the vertical gun is already dropping in intensity. While vacuum was also broken for the horizontal scanner, it didn't suffer from the same suspected problem, cathode poisoning. Because the cathode is made of LaB6, extra heating of the cathode can reduce the poisoning and improve the cathode's emission.

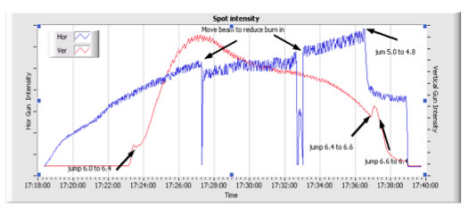

Figure 12: Cathode performance after breaking vacuum.

ISBN 978-3-95450-118-2

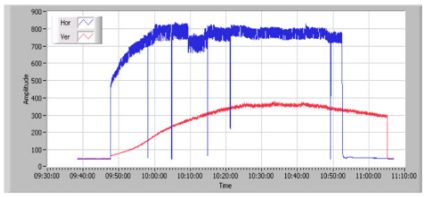

Figure 13: Cathode performance after pre-heating.

We found that heating the cathode at higher than normal settings and, specifically, also keeping the accelerating voltage off, improved the cathode's performance, see Fig. 13. The pre-heating is now standard and has actually increased the cathode's emission relative to before the vacuum break. Higher heating current could further improve the cathode's emission, but we don't want to risk a catastrophic failure by either burning up the cathode heater or cracking the gun.

Unwanted Illumination

In both planes, we can see lines or blobs of unwanted electrons illuminating the screen, see Fig. 14. These unwanted electrons impede the analysis and/or result in an additional bump in the derived profile.

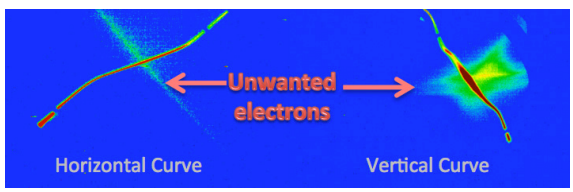

Figure 14: Unwanted electrons illuminate the screen.

The unwanted electrons are thought to originate right before and right after the scan. Figure 15 shows the deflector voltages (orange and dark blue) and the accelerating High Voltages (HV) (red and light blue) for both planes. Most of the unwanted electrons can be scraped away by setting the optics such that the electrons from before and after the scan hit the beam pipe before reaching the screen. However, focusing by the proton beam and the fall-off of the deflector voltage during the HV pulse is thought to allow for the electrons to reach the screen.

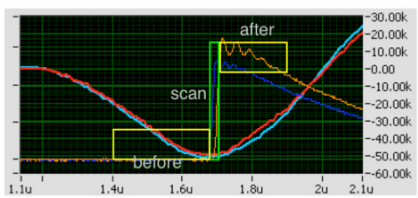

Figure 15: The scanner's voltage waveforms.

Additional scraping of the electrons could reduce this problem. Luckily, the electron scanner has two vacuum valves, one on each side of the ring beam pipe, see Fig. 2, which can be used to scrape beam even if it is just on one side at the time. The electron gun was set up to show the unwanted electrons. By very slowly closing either the upstream or downstream valve, electrons were scraped. Figure 16 shows that the valves visibly scraped the unwanted electrons from different directions. Even though the valves also scraped part of the wanted electrons, the results are encouraging and we will add scrapers or an aperture restriction in the future.

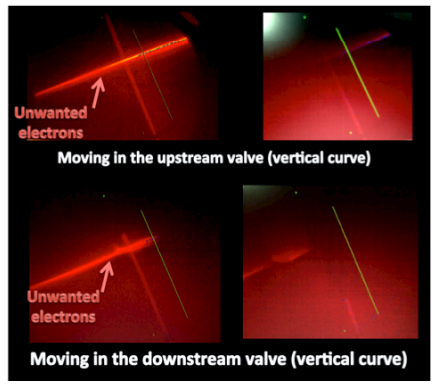

Figure 16: Scraping the electron beam with the vacuum valves.

TARGET IMAGING SYSTEM

During this past summer's maintenance period, both the proton window, on which a TIS mirror is mounted, and the target were replaced. During this installation, a remote controllable lamp was installed. The lamp can illuminate the coating thus avoiding the need for beam time.

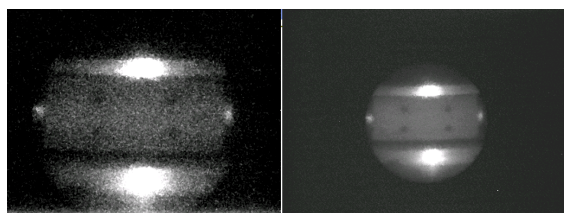

Figure 17: View of the target coating using the lamp.

Figure 17 shows the images obtained with the current camera, a GC1290, on the left. The image is not bright enough and too grainy to make a good calibration. On the right is the image from the AVT G-145B. This camera is more sensitive and does provide an image useable for calibration. This camera will be used once we adapt the final focusing lens to fully use its sensor area.

FOIL IMAGING SYSTEM

The radiation at the stripper foil is very high due to the beam losses that occur as part of the stripping process. The analog camera is placed in a cubbyhole in the wall but still receives radiation doses of up to 20 kRad per month. The analog camera's exposure cannot be adjusted and is too long compared to the beam pulse duration to do temperature measurements. It is also not sensitive enough to make the foil visible under some conditions, even when the foil lamp is turned on. While non-radhard digital cameras do survive for several months in the same location, they lock up, at best, in a matter of minutes and thus require continuous reboots. An initial attempt to

ISBN 978-3-95450-118-2

measure the foil temperature with cameras in the tunnel failed as they locked up too quickly.

We found a suitable optical path through an unused cable chase to guide the light from the tunnel to a service building using only two mirrors. This new optical path now provides us with a platform to test digital cameras and develop temperature measurements. The test setup already displays the foil in the control room without having to turn the lamp on, see Fig. 18. The display combines two images with different exposures, one long exposure to make the foil visible and one short exposure to show the beam wherever the long exposure image is saturated. Heat turbulence and vibrations affect the stability of the image. We plan to counter this by placing a shield and a fan over the beam pipe to disperse the heat from the magnets and by improving the telescope stand.

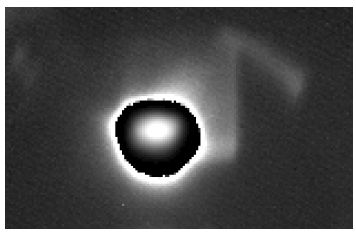

Figure 18: Composite image of the stripper foil.

Replacing the digital camera with an electrically shielded eyepiece holding a photodiode with interchangeable bandpass filters implements a two-color pyrometer, see Fig. 19.

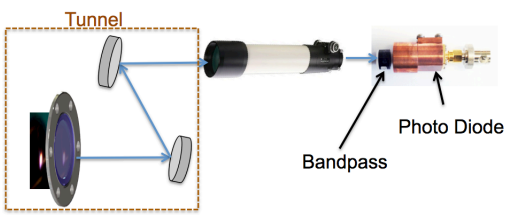

Figure 19: Foil temperature measurement setup.

Two different bandpass filters, 1050 nm and 1600 nm, were placed in front of the photodiode, one at time, for an initial test. Figure 20 shows the resulting signals after amplification. The waveforms show the 1 ms linac pulse heating the foil and a subsequent cool down over about 10 ms. The temperature can be calculated by taking the ratio of the two signals. However, in our case we have not yet limited the light to a certain location on the foil. As such, the signals represent a mix of temperatures. Filtering can further improve the signal to noise ratio, which will be needed once we limit the light to a section of the foil. A software program is under development to take the photodiode's signal and the optical characteristics of the filter, photodiode, and other optical elements to calculate the foil temperature. A computerized telescope mount has already been installed so that we can scan the foil and measure the temperature as a function of the foil location.

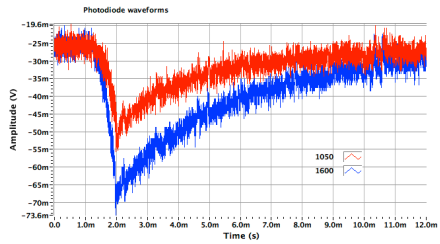

Figure 20: Photodiode signals.

SUMMARY

We are making progress in improving the electron scanner; the range has been improved, the vertical profile cathode's current is higher, and soon we hope to significantly reduce the unwanted electrons. A method to derive the transverse profile of a short bunch has been proposed. The added lamp to the TIS system will make pre-beam calibration possible when we upgrade to the new camera. The optical path guiding the stripper foil's light to outside the radiation area has provided us with a test platform to make temperature measurements and provide a better image of the foil.

ACKNOWLEDGEMENTS

Many people have contributed to the presented work. The author would like to thank in particular: R.W. Dickson, L. Yun, H. Chunning, L.C. Maxey, and I.N. Nesterenko for their optics work on the FIS, J.G. Janney, R.F. Conn, P.W. Walker, L.C. Maxey, T.J. Shea, and T.J McManamy for their work on the TIS, as well as A. Webster, J.W. Diamond, and S.N. Murray for their technical work on all systems. The author also thanks the ProjectX collaboration for its support.

REFERENCES

[1] W. Blokland, "Non-Invasive Beam Profile Measurements Using An Electron-Beam Scanner," Proc. HB 2010, Morschach, Switzerland, pp. 438-442.

[2] W. Blokland and S. Cousineau, "A Non-Destructive Profile Monitor For High Intensity Beams," Proc. 2011 PAC, New York, NY, USA, pp. 1438-44.

[3] T. J. Shea, et. al., "Installation and Initial Operation of an On-line Target Imaging System for SNS," ICANS XIX (2010), New Orleans, LA, USA, pp. 882-4.

[4] M.A Plum, J. Holmes, R.W. Shaw, and C.S. Feigerle, "SNS Stripper Foil Development Program," *Nucl. Instrum. Methods Phys. Resh. A*, 590, 43-46 (2008).

[5] P.V. Logachev, D.A. Malyutin, A.A. Starostenko, "Application of a low-energy electron beam as a tool of nondestructive diagnostics of intense charged-particle beams," Instruments and Experimental Techniques, Volume 51, Number 1 (2008).

[6] W. Blokland, "Fitting RTBT Beam Profiles: the case for the Super-Gaussian," Internal Memo, SNS/RAD, ORNL, Nov 2009.

ISBN 978-3-95450-118-2